Eur. Phys. J. D **38**, 15–20 (2006)
DOI: 10.1140/epjd/e2006-00018-2

THE EUROPEAN PHYSICAL JOURNAL D

Probing spin-orbit quenching in Cl (^{2}P) + H_2 via crossed molecular beam scattering

B.F. Parsons, K.E. Strecker, and D.W. Chandler[a]

Combustion Research Facility, Sandia National Laboratory, 7011 East Ave., Livermore, CA 94550, USA

Received 17 August 2005 / Received in final form 2nd December 2005
Published online 31 January 2006 –

Abstract. In our previous work we investigated electronically non-adiabatic effects in Cl ($^2P_{3/2,1/2}$) + D_2 using crossed molecular beam scattering coupled with velocity mapped ion imaging. The prior experiments placed limits on the cross-section for electronically non-adiabatic spin-orbit excitation Cl ($^2P_{3/2}$) + D_2 → Cl* ($^2P_{1/2}$)+D_2 and electronically non-adiabatic spin-orbit quenching Cl* ($^2P_{1/2}$)+D_2 → Cl ($^2P_{3/2}$)+D_2. In the present work, we investigate electronically non-adiabatic spin-orbit quenching for Cl* ($^2P_{1/2}$) + H_2 which is the required first step for the reaction of Cl* to produce ground state HCl + H products. In these experiments we collide Cl (^{2}P) with H_2 at a series of fixed collision energies using a crossed molecular beam machine with velocity mapped ion imaging detection. Through an analysis of our ion images, we determine the fraction of electronically adiabatic scattering in Cl* + H_2, which allows us to place limits on the cross-section for electronically non-adiabatic scattering or *quenching*. We determine the following quenching cross-sections σ_{quench}(2.1 kcal/mol) = 26 ± 21 Å^2, σ_{quench}(4.0 kcal/mol) = 21 ± 49 Å^2, and σ_{quench}(5.6 kcal/mol) = 14 ± 41 Å^2.

PACS. 34.50.Lf Chemical reactions, energy disposal, and angular distribution, as studied by atomic and molecular beams – 34.50.Pi State-to-state scattering analyses – 34.50.-s Scattering of atoms and molecules

1 Introduction

The Cl + H_2 reaction serves as an archetype for the reaction of atomic chlorine with hydrocarbons; such reactions are important in atmospheric and combustion chemistry [1]. The contribution of spin-orbit excited atomic chlorine, Cl* ($^2P_{1/2}$), to the Cl + H_2 → HCl + H reaction currently remains one of the most important unresolved topics in gas phase physical chemistry. In Figure 1 we summarize the salient details of the lowest potential energy surfaces (PESs) for Cl ($^2P_{3/2,1/2}$) + H_2 in a linear geometry. For a large separation between the Cl atom and the H_2 center-of-mass, the ground electronic state is doubly degenerate. Reaction to form HCl ($^1\Sigma^+$) + H (^{2}S) takes place on the $^2\Sigma^+_{1/2}$ PES. The overall Cl + H_2 → HCl + H reaction is slightly endothermic with $\Delta H = 1.06$ kcal/mol. The $^2\Pi_{3/2}$ ground state surface correlates with higher energy HCl (a $^3\Pi$) + H (^{2}S) products as does the $^2\Pi_{1/2}$ PES corresponding to a Cl* ($^2P_{1/2}$) + H_2collision. These excited state products are not accessible at moderate collision energies ($\lesssim$10 kcal/mol).

In the Born-Oppenheimer approximation, with no coupling between the $^2\Pi_{1/2}$ potential energy surface and the doubly degenerate ground state potential energy surface, Cl*+ H_2 is non-reactive. Therefore both the $^2\Pi_{3/2}$ PES and the $^2\Pi_{1/2}$ PES shown in Figure 1 should result in electronically adiabatic scattering at moderate collision energies. Recent theoretical calculations by Alexander and co-workers [2,3] find that the spin-orbit energy from Cl* couples inefficiently into the formation of ground state reaction products which supports the notion of weak coupling between the excited and ground

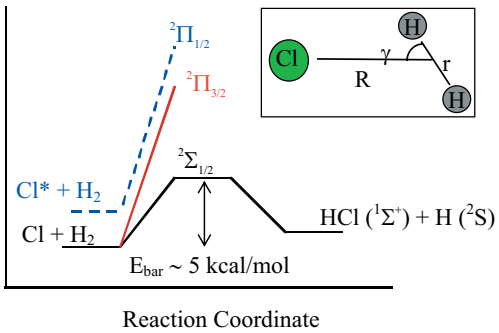

Fig. 1. Potential energy surfaces for Cl (^2P_j) + H_2. In the Born-Oppenheimer approximation only the $^2\Sigma_{1/2}$ state leads to formation of ground state products.

[a] e-mail: chand@sandia.gov

state Born-Oppenheimer PESs. Thus, only at collision energies below the reaction barrier on the $^2\Sigma^+_{1/2}$ surface ($\lesssim$5 kcal/mol) does Cl^* + H_2 contribute significantly to the overall reaction since at collision energies below the barrier the spin-orbit energy (∼2.5 kcal/mol) is available to surmount the reaction barrier. However, as the collision energy increases above the energy of the barrier, the contribution from the $^2\Sigma^+_{1/2}$ PES increases rapidly and dominates the overall reaction [2,3].

Several experimental studies show remarkable consistency with theoretical predictions using the latest potential energy surfaces for Cl + H_2. In particular, the angular distributions calculated from the potential energy surfaces for Cl + H_2 show good agreement with the measurements of Casavecchia and co-workers [4]. Furthermore, the kinetics of Cl + H_2 now show remarkably good agreement between theory [5] and experiments [6]. Even the HCl/DCl branching ratio for the Cl + HD molecular beam experiments is well reproduced due to the inclusion of a shallow van der Waal's well in the entrance channel of the potential energy surface [7].

On the other hand, there is considerable experimental evidence that Cl^* + H_2 dominates this reaction at collision energies well above the reaction barrier on the $^2\Sigma^+_{1/2}$ PES [8–10]. In order for Cl^* to contribute to reaction forming ground state products the reactants must first undergo an electronically non-adiabatic transition to the reactive ground state PES. The notion of a facile electronically non-adiabatic transition between the $^2\Pi_{1/2}$ and the $^2\Sigma^+_{1/2}$ PES is not consistent with small coupling between these two Born-Oppenheimer surfaces. During an electronically non-adiabatic transition the spin-orbit energy is deposited into relative translation of the reactants or H_2 internal rotation. The final form of the energy may enhance the reaction as in the case of relative translation [8]. The influence of H_2 internal rotation has been considered for some lower H_2 rotational levels [2,8].

A related reaction, F + H_2, has received a considerable amount of attention as [11–13]. The F + H_2 reaction is highly exothermic (ΔE = 32.0 kcal/mol) unlike Cl + H_2, which is slightly endothermic *vide supra.* However, for both of these systems X + H_2 reactants lead to ground state HX + H products while reaction forming ground state products is Born-Oppenheimer forbidden for X^* + H_2. Therefore, for either system the formation of ground state products from spin-orbit excited reactants is due to electronically non-adiabatic effects. Of particular relevance to our work on non-adiabatic interactions in Cl + H_2, Nesbitt and co-workers [13] studied non-adiabatic interactions in F + H_2 at collision energies well below the ground state reaction barrier of 1.9 kcal/mol. At center-of-mass collision energies of 0.54 kcal/mol, Nesbitt and co-workers observed HF (v = 3, J = 3–5) products that are energetically forbidden for the Born-Oppenheimer allowed F + H_2 channel. Since F^* + H_2 can form HF (v = 3, J = 3–5) at this collision energy, the observation of higher energy products as well as the observation of a significant reactive cross-section for F + H_2 well below the energy of the ground state barrier provided evidence for a contribution of F^* to the overall reaction. More recently, Alexander et al. have determined that the Born-Oppenheimer forbidden channel in F + H_2 contributes at most ∼25% to the overall reaction [14]. In their work on F + H_2, Alexander et al. calculated the cross-section for the near-resonant energy transfer process F^* + H_2 (J = 0) → F + H_2 (J = 2) for which ΔE = −0.121 kcal/mol. Their calculations show the cross-section for this quenching process drops monotonically from $\sigma \sim 40$ Å^2 at ∼0 kcal/mol collision energy to $\sigma \sim 12$ Å^2 for collision energies near the barrier to reaction (∼1.9 kcal/mol) [14].

In this paper, we investigate the quenching of Cl^* following a collision with H_2 at several collision energies spanning the energy for the reaction barrier in the $^2\Sigma^+_{1/2}$ state. In the next section we provide a brief review of the experimental technique we developed to look at quenching in Cl + D_2 [15]. In Section 3 we discuss the important results from characterization of our atomic and molecular beams as well as the results from our imaging experiments, which give the effective quenching probability for Cl^* + H_2. In Section 4 we discuss the quenching probability for Cl^* + H_2 at the collision energies sampled by our molecular beam experiments. Furthermore, we address the differences that arise between the quenching of Cl^* in the molecular beam experiments and in the supersonic expansion. The final section of this paper briefly summarizes the key points and presents a conclusion.

2 Experimental

These experiments use the same technique that we previously developed for an investigation of the electronically non-adiabatic scattering in Cl^* + D_2 [15]. In these experiments, we form an atomic beam of Cl/Cl^* through photolysis of Cl_2 at 420 nm by focusing a laser (Coherent Infinity Nd:YAG/OPO, 3 ns pulse) at the throat of a supersonic expansion of ∼5% Cl_2 in a carrier gas (Ar, He, or H_2). Atomic Cl then collides with H_2 from a supersonic expansion of neat H_2. Both molecular beams are formed using piezoelectric valves [16]. The molecular beams counterpropagate giving a collision geometry of 180°. We state-selectively ionize atomic Cl or Cl^* using resonance enhanced multiphoton ionization (REMPI) [10]. The CI^+ ions are detected using velocity mapped ion imaging [17].

For these experiments, we collect data by collecting pairs of ion images. Each pair of ion images has one image with Cl/Cl^* and the H_2 collider beams overlapped in time and one image with the H_2 delayed in time and only Cl/Cl^* present. After collecting each of the two individual images for 2–5 s we subtract the Cl/Cl^* only image from the Cl/Cl^* + H_2 image and repeat this process ∼30–60 times. In the Cl/Cl^* only image, the atomic beam spot is slightly more intense because no Cl/Cl^* has been lost due to scattering with H_2. Figure 2 shows the result when we subtract the Cl only ion image from the Cl + H_2 ion

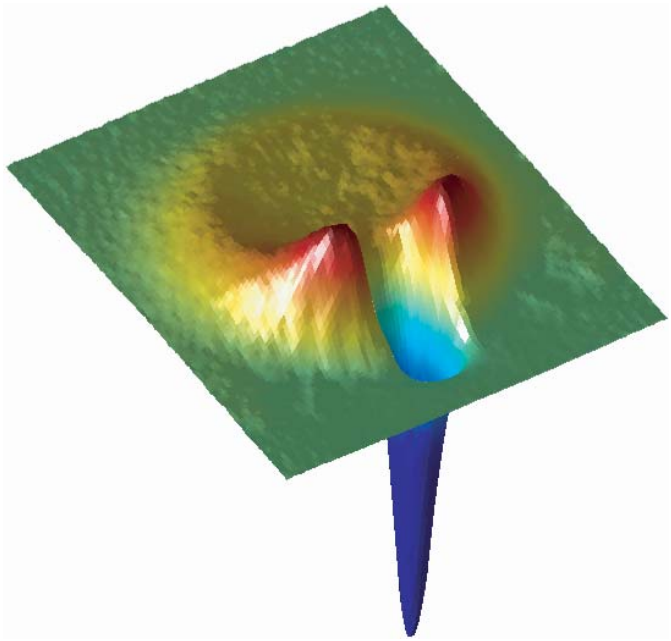

Fig. 2. Example ion image for Cl + H_2 scattering after subtraction of the unscattered Cl beam spot. The dominant circular ridge in the front of the image is forward scattered Cl resulting from electronically adiabatic rotationally elastic collisions with H_2. The large negative dip in the image corresponds to the amount of Cl scattered out of the atomic beam. A color version of the figure is available in electronic form at `http://www.eurphysj.org`.

image. The image in Figure 2 has two important features. First, we see Cl that was scattered out from the atomic beam and detected by the experiment as a positive ring in this image. Second, after subtraction the atomic beam spot appears as a large negative region in the image. In Section 3 we discuss how our data analysis of these images proceeds. During these experiments we insure that the position sensitive ion detector is not saturated after collecting each data set.

3 Results

The ion images presented in this paper have two features that we use to determine the probability for electronically adiabatic scattering. In Figure 2, we show an example of a subtracted ion image for Cl + H_2. As discussed above, the forward scattered circular ridge corresponds to Cl from electronically adiabatic scattering while the negative spike in the image corresponds to Cl scattered out of the atomic beam. We list below the scattering processes that may take place in our experiments:

$$\mathrm{Cl/Cl^*} + \mathrm{H_2}\ (v=0, J'') \rightarrow \mathrm{Cl/Cl^*} + \mathrm{H_2}\ (v=0, J') \quad (1a)$$

$$\mathrm{Cl/Cl^*} + \mathrm{H_2} \rightarrow \mathrm{HCl} + \mathrm{H} \quad (1b)$$

$$\mathrm{Cl^*/(Cl)} + \mathrm{H_2} \rightarrow \mathrm{Cl/(Cl^*)} + \mathrm{H_2}. \quad (1c)$$

Process (1a) is electronically adiabatic scattering; this type of scattering includes both rotationally elastic ($J'' = J'$) and inelastic scattering ($J'' < J'$) with no change in the internal Cl state — this is the only type of scattering that shows up in our images. Process (1b) is reactive scattering, which leads to a loss of Cl from the beam spot with no corresponding scattered Cl appearing in the image. Because the cross-section for reactive scattering (1b), is much smaller than that for electronically adiabatic scattering, equation (1b), we can safely neglect process (1b) [15]. Process (1c) corresponds to electronically non-adiabatic scattering resulting in a change of the electronic state of atomic chlorine during the collision. We wish to determine the size of electronically non-adiabatic scattering, process (1c), relative to that for electronically adiabatic scattering. The magnitude of electronically non-adiabatic quenching can be determined by finding out how much Cl* has been lost from the atomic beam and how much Cl* appears as electronically adiabatic scattering.

Different regions of our state-selected velocity mapped ion images correspond to nascent Cl (or Cl*) in the atomic beam and Cl (or Cl*) scattered out of the beam. We analyze the ion images in the following manner. First the total scattered Cl (or Cl*) in each image (red/brown regions in Fig. 2) is integrated to give the amount of electronically adiabatic scattering, $I^{H_2}_{EA,exp}(\mathrm{Cl/Cl^*})$. The total amount of Cl (or Cl*) lost from the atomic beam, $I^{H_2}_{L,exp}(\mathrm{Cl/Cl^*})$, is determined by integrating the negative area in each image (negative spike in Fig. 2). The fraction of detected Cl (or Cl*) that is lost from the atomic beam and results in electronically adiabatic elastic scattering is given as:

$$f^{H_2}_{EA,exp}(\mathrm{Cl/Cl^*}) = I^{H_2}_{EA,exp}(\mathrm{Cl/Cl^*})/I^{H_2}_{L,exp}(\mathrm{Cl/Cl^*}). \quad (2)$$

If all of the Cl/Cl* lost from the atomic beam resulted in electronically adiabatic elastic scattering and both the scattered and lost Cl (or Cl*) are detected with equal efficiency then $f^{H_2}_{EA,exp}(\mathrm{Cl/Cl^*}) = 1$. A deviation of $f^{H_2}_{EA,exp}(\mathrm{Cl/Cl^*})$ from unity could result from a loss Cl* due to electronically non-adiabatic scattering *vide supra*. Alternatively, a deviation in $f^{H_2}_{EA,exp}(\mathrm{Cl/Cl^*})$ from unity may result from differences in the detection efficiency for unscattered versus scattered Cl/Cl*, that is a difference in detection for state-selected Cl or Cl* the atomic beam versus the detection efficiency for electronically adiabtiacally scattered Cl or Cl*.

Since we use 2+1 REMPI to state-select Cl or Cl*, the detection efficiency varies with the square of the ionization laser power. The ionization laser is focused on the crossing between our atomic Cl beam and the H_2 beam; however, scattered Cl/Cl* flies out of the interaction region while nascent Cl/Cl* does not. Hence, scattered and unscattered Cl/Cl* experience different laser intensities and have different ionization and detection efficiency. As in our previous experiments, we account for the different detection efficiency for scattered Cl/Cl* and uncollided Cl/Cl* by utilizing the fact that the velocity and angular distribution for scattered Cl and for scattered Cl* are identical within the sensitivity of our experiment. Since we use the same laser power and focusing for both Cl and Cl*, the detection efficiency for scattered Cl and Cl* are the same

as are the detection efficiency for nascent Cl and Cl^*. Furthermore, reaction (1b) does not account for a significant loss of Cl and we observe no electronically non-adiabatic spin-orbit excitation, $Cl + H_2 \rightarrow Cl^* + H_2$, in our images. With no significant pathway leading to loss of Cl we can state that the probability for electronically adiabatic scattering for $Cl + H_2$ is one, $f^{H_2}_{EA,true}(Cl) = 1$. Under this assumption the measured ratio $f^{H_2}_{EA,exp}(Cl)/f^{H_2}_{EA,true}(Cl)$ is then a measure of the ratio of the detection efficiency for scattered and nascent Cl and will be used to normalize the Cl^* quenching data.. We use this ratio to correct the measured fraction of electronically adiabatic scattering in Cl^* giving $f^{H_2}_{EA,corrected}(Cl^*)$.

From our measurement of the electronically adiabatic branching fraction, we can estimate the cross-section for electronically non-adiabatic quenching. To do this we first note that two main processes contribute to the scattering of Cl^* from the atomic beam — electronically adiabatic scattering (Eq. (1a)) and electronically non-adiabatic scattering (Eq. (1c)). Electronically adiabatic scattering includes both rotationally elastic and rotationally inelastic scattering; however, the process outlined in equation (1a) is dominated by elastic scattering. For Cl (^{2}P) + D_2, we previously estimated the cross-section for elastic scattering to be $\sigma_{EA} \sim 100$ Å^2 [15]. Our previous estimate for the elastic scattering cross-section and the electronically adiabatic cross-section should be approximately correct for $Cl + H_2$. Since we have only two competing processes the upper limit for the quenching cross-section may be expressed as:

$$\sigma_{ENA} \leq \frac{f^{H_2}_{ENA,corrected}(Cl^*)}{f^{H_2}_{EA,corrected}(Cl^*)}\sigma_{EA} \approx \frac{1 - f^{H_2}_{EA,corrected}(Cl^*)}{f^{H_2}_{EA,corrected}(Cl^*)}\sigma_{EA} \quad (3)$$

where σ_{ENA} and σ_{EA} are the electronically non-adiabatic scattering cross-section and electronically adiabatic scattering cross-sections respectively and $f^{H_2}_{ENA,corrected}(Cl^*)$ and $f^{H_2}_{EA,corrected}(Cl^*)$ are the corrected fractions of Cl^* lost from the atomic beam due to electronically non-adiabatic scattering (Eq. (1c)) and electronically adiabatic scattering (Eq. (1a)).

We have measured the fraction of electronically adiabatic scattering for $Cl^* + H_2$ at three collisions energies (2.1, 4.0, and 5.6 kcal/mol) that span the energetic height for the reaction barrier on the ground electronic state. We obtain the following results from these measurements. At the lowest collision energy, 2.1 kcal/mol (using Ar as the Cl_2 seed gas) we find the electronically adiabatic branching fraction to be $f^{H_2}_{EA,corrected}(Cl^*) = 0.79 \pm 0.17$ and the corresponding quenching cross-section found using equation (3) is 26 ± 21 Å^2. For $Cl^* + H_2$ collisions at 4.0 kcal/mol (using He as the Cl_2 seed gas) we measure the $f^{H_2}_{EA,corrected}(Cl^*) = 0.83 \pm 0.38$ and the corresponding quenching cross-section to be 21 ± 49 Å^2. Finally, for the highest collision energy studied, 5.7 kcal/mol (using H_2 as the Cl_2 seed gas) we measure the $f^{H_2}_{EA,corrected}(Cl^*) = 0.88 \pm 0.35$ and the corresponding quenching cross-section to be 14 ± 41 Å^2. These results are summarized in Table 1. We note that as the collision energy increases the amount of non-adiabatic behavior decreases. We discuss below that this is consistent with $F^* + H_2$ calculations and not the way a Landau-Zener type avoided curve crossing would behave.

Table 1. We give the fraction of electronically adiabatic scattering for $Cl^* + H_2$ as a function of collision energy. We also give the electronically non-adiabatic scattering cross-section determined using equation (3).

Seed gas	T_{col}(kcal/mol)	$f^{H_2}_{EA,corrected}(Cl^*)$	σ (Å^2)
Ar	2.1	0.79 ± 0.17	26 ± 21
He	4.0	0.83 ± 0.38	21 ± 49
H_2	5.6	0.88 ± 0.35	14 ± 41

Finally, for comparison, we have repeated our previous experiment to measure the quenching in $Cl^* + D_2$ at a single collision energy (7.6 kcal/mol). Since these experiments require only that we change the collider gas from H_2 to D_2, we can perform the both the H_2 and D_2 experiments back-to-back. By doing this we can reference our current results with those in the previous study. At this collision energy, we previously measured the electronically adiabatic scattering fraction to be 0.78 ± 0.22 which compares reasonably very well with our current measurement of $f^{H_2}_{EA}(Cl) = 0.92 \pm 0.27$.

4 Discussion

4.1 Electronically non-adiabatic scattering cross-sections

In this experiment, we determine the electronically non-adiabatic quenching cross-section for $Cl^* + H_2$. The cross-section for quenching in this system varies between 26 ± 21 Å^2 at 2.0 kcal/mol to 21 ± 49 Å^2 at 4.0 kcal/mol to 14 ± 41 Å^2 at 5.7 kcal/mol. The uncertainty in the fraction of quenching is the same as the uncertainty in the fraction of electronic adiabatic scattering. Since the total amount of quenching ($1 - f^{H_2}_{EA,exp}(Cl^*)$) is small the relative error in the denominator of equation (3) is quite large. This results in the large error bars for the quenching cross-section given above.

It is useful to compare our measurement for the electronically non-adiabatic scattering cross-section for $Cl^* + H_2$ to the cross-section calculated by Alexander et al. for $F^* + H_2$ ($J = 0$) $\rightarrow F + H_2$ ($J = 2$) [14]. As we discussed above, Alexander et al. calculated the electronically non-adiabatic scattering cross-section as 40 Å^2 at near zero collision energy and the cross-section for quenching decreases monotonically as collision energy increases reaching a value of ∼10–15 Å^2 for collision energies near the ground state reaction barrier (∼1.9 kcal/mol). As a comparison, for $T_{col} \sim 2$ kcal/mol the reaction cross-section

for F + H_2 ($J = 0$) is ∼2 Å^2. However, the calculations of Alexander et al. give the reactivity of spin-orbit excited F* as ≥25% of the reactivity of [14]. For Cl* + H_2 we estimate the total quenching cross-section to be ∼25 Å^2 which is similar to that for F* + H_2 although the reactive cross-section for Cl + H_2 is calculated to be ∼0.1 Å^2 [2]. For the chlorine reaction the contribution of Cl* + H_2 to the reaction has been calculated to be quite small for energies above the barrier on the reactive ground state [2].

4.2 Quenching mechanism

In order for Cl* to quench effectively to the ground state during a collision with H_2 a near-resonant energy transfer process similar as F* + H_2 ($J = 0$) → F + H_2 ($J = 2$) [11,14] may be responsible. One likely process for Cl* + H_2 is:

$$\mathrm{Cl}^* + \mathrm{H_2}(J=2) \rightarrow \mathrm{Cl} + \mathrm{H_2}(J=4) \qquad \Delta E = -0.09 \text{ kcal/mol} \quad (4a)$$

where $\Delta E = E_{SO} - E_{rot}$. The only other process with a small value of ΔE is:

$$\mathrm{Cl}^* + \mathrm{H_2}(J=1) \rightarrow \mathrm{Cl} + \mathrm{H_2}(J=3) \qquad \Delta E = -0.78 \text{ kcal/mol.} \quad (4b)$$

The $|\Delta E|$ for equation (4b) is large enough to make this non-resonant while (4a) is fairly close to resonant energy transfer. Therefore, process (4a) can dominate Cl* + H_2 quenching in our molecular beam experiment.

We can consider the near resonant energy transfer processes that could lead to the quenching in Cl* + D_2 studied in our previous work [15]. The processes that is closest to resonant are:

$$\mathrm{Cl}^* + \mathrm{D_2}(J=1) \rightarrow \mathrm{Cl} + \mathrm{D_2}(J=5) \qquad \Delta E = -0.08 \text{ kcal/mol} \quad (5a)$$

$$\mathrm{Cl}^* + \mathrm{D_2}(J=5) \rightarrow \mathrm{Cl} + \mathrm{D_2}(J=7) \qquad \Delta E = -0.26 \text{ kcal/mol} \quad (5b)$$

$$\mathrm{Cl}^* + \mathrm{D_2}(J=4) \rightarrow \mathrm{Cl} + \mathrm{D_2}(J=6) \qquad \Delta E = -0.61 \text{ kcal/mol.} \quad (5c)$$

Process (5a) is quite close to resonant but involves a large change in rotational quantum number $\Delta J = +4$. Both process (5b) and (5c) require higher rotational states of D_2, which have low populations at 300 K and in our cooled molecular beams. Process (5a) is likely the dominant quenching mechanism for Cl* + D_2 given the near resonant energy transfer and the large population of $D_2(J = 1)$. However, we previously observed very little quenching for Cl* + D_2 in molecular beam experiments [15]. The large change in rotational quantum number most likely accounts for the lower quenching of D_2 relative to H_2. However, theoretical calculations for the quenching cross-sections for Cl* by H_2 and D_2 are needed to resolve the mechanism through which quenching proceeds in these two systems.

5 Conclusions

We have investigated the propensity for an electronically non-adiabatic spin-orbit quenching collision in Cl* + H_2 using crossed molecular beam scattering coupled with ion imaging detection. Our experiment determines the total amount of Cl (^{2}P) that is lost from our atomic beam due to collisions with H_2 and the fraction of Cl (^{2}P) that appears as electronically adiabatic scattering. Any Cl* not accounted for in our experiment corresponds to a loss due to electronically non-adiabatic scattering, *quenching*. We determine the following quenching cross-sections for Cl* + H_2: 26 ± 21 Å (2.1 kcal/mol), 21 ± 49 Å (4.0 kcal/mol), and 14 ± 41 Å (5.7 kcal/mol). These quenching cross-sections are similar in magnitude to the quenching cross-section calculated for F* + H_2 (∼12 Å^2 at a collision energy near the energetic barrier to reaction for F + H_2). In the F + H_2 reaction it is well understood that the contribution of F* to the total reaction is small ≤25% [14]. In analogy with F* + H_2 a likely quenching mechanism in Cl* + H_2 results from the near resonant spin-orbit to rotational energy transfer process: Cl* + $H_2(J = 2)$ → Cl + $H_2(J = 4)$. A similar near resonant process seems unlikely for Cl* + D_2.

We would like to thank Mr. Mark Jaska for valuable technical assistance. We would also like to express our thanks to Dr. Jaime Ramirez-Serrano for valuable discussions and assistance. This research is supported by the Division of Chemical Sciences, Geosciences, and Biosciences, the Office of Basic Energy Sciences of the U.S. Department of Energy. Sandia is a multi-program laboratory operated by Sandia Corporation, a Lockheed Martin Company, for the United States Department of Energy's National Nuclear Security Administration under contract DE-AC04-94AL85000.

References

1. H.A. Michelsen, W.R. Simpson, J. Phys. Chem. A **105**, 1476 (2001); S.M. Senkan, J.M. Robinson, A.K. Gupta, Combust. Flame **49**, 305 (1983)
2. M.H. Alexander, G. Capecchi, H.J. Werner, Science **296**, 715 (2002)
3. M.H. Alexander, G. Capecchi, H.-J. Werner, Faraday Discuss. **127**, 59 (2004)
4. N. Balucani, D. Skouteris, L. Cartechini, G. Capozza, E. Segoloni, P. Casavecchia, M.H. Alexander, G. Capecchi, H.-J. Werner, Phys. Rev. Lett. **91**, 013201 (2003)
5. U. Manthe, W. Bian, H.-J. Werner, Chem. Phys. Lett. **313**, 647 (1999); U. Manthe, G. Capecchi, H.-J. Werner, Phys. Chem. Chem. Phys. **6**, 5026 (2004)
6. S.S. Kumaran, K.P. Lim, J.V. Michael, J. Chem. Phys. **101**, 9487 (1994); C.A. Taatjes, Chem. Phys. Lett. **306**, 33 (1999)
7. D. Skouteris, D.E. Manolopoulos, W. Bian, H.-J. Werner, L.-H. Lai, K. Liu, Science **286**, 1713 (1999)
8. S.-H. Lee, L.-H. Lai, K. Liu, H. Chang, J. Chem. Phys. **110**, 8229 (1999)
9. S.-H. Lee, K. Liu, J. Chem. Phys. **111**, 6253 (1999)

10. F. Dong, S.-H. Lee, K. Liu, J. Chem. Phys. **115**, 1197 (2001)
11. F. Rebentrost, J. Lester, J. Chem. Phys. **67**, 3367 (1977); R.E. Wyatt, R.B. Walker, J. Chem. Phys. **70**, 1501 (1979)
12. D.M. Neumark, A.M. Wodtke, G.N. Robinson, C.C. Hayden, Y.T. Lee, Phys. Rev. Lett. **53**, 226 (1984); D.M. Neumark, A.M. Wodtke, G.N. Robinson, C.C. Hayden, Y.T. Lee, J. Chem. Phys. **82**, 3045 (1985); W.B. Chadman, B.W. Blackmon, D.J. Nesbitt, J. Chem. Phys. **107**, 8193 (1997); F. Dong, S.-H. Lee, K. Liu, J. Chem. Phys. **113**, 3633 (2000); S.A. Nizkorodov, W.W. Harper, W.B. Chapman, B.B. Blackmon, D.J. Nesbitt, J. Chem. Phys. **111**, 8404 (1999); D.E. Manolopoulos, J. Chem. Soc. Faraday Trans. **93**, 673 (1997)
13. S.A. Nizkorodov, W.W. Harper, D.J. Nesbitt, Faraday Disscus. Chem. Soc. **113**, 107 (1999)
14. M.H. Alexander, D.E. Manolopoulos, H.-J. Werner, J. Chem. Phys. **113**, 11084 (2000)
15. B.F. Parsons, D.W. Chandler, J. Chem. Phys. **122**, 174306 (2005)
16. D. Proch, T. Trickl, Rev. Sci. Instrum. **60**, 713 (1989)
17. D.W. Chandler, P.L. Houston, J. Chem. Phys. **87**, 1445 (1987); D.H. Parker, A.T.J.B. Eppink, J. Chem. Phys. **107**, 2357 (1997)